

Metabolic Analysis of the Synthesis of High Levels of Intracellular Human SOD in *Saccharomyces cerevisiae* rhSOD 2060 411 SGA122

Ramon Gonzalez,* Barbara A. Andrews, Julia Molitor, Juan A. Asenjo

Centre for Biochemical Engineering and Biotechnology, Department of Chemical Engineering, Millennium Institute for Advanced Studies In Cell Biology and Biotechnology, University of Chile, Beauchef 861, Santiago, Chile; telephone: 56-2-6784288; fax: 56-2-6991084; e-mail: juasenjo@cec.uchile.cl

Received 31 January 2002; accepted 18 September 2002

DOI: 10.1002/bit.10556

Abstract: The synthesis of human superoxide dismutase (SOD) in batch cultures of a *Saccharomyces cerevisiae* strain using a glucose-limited minimal medium was studied through metabolic flux analysis. A stoichiometric model was built, which included 78 reactions, according to metabolic pathways operative in these strains during respirofermentative and oxidative metabolism. It allowed calculation of the distribution of metabolic fluxes during diauxic growth on glucose and ethanol. Fermentation profiles and metabolic fluxes were analyzed at different phases of diauxic growth for the recombinant strain (*P+*) and for its wild type (*P-*). The synthesis of SOD by the strain *P+* resulted in a decrease in specific growth rate of 34 and 54% (growth on glucose and ethanol respectively) in comparison to the wild type. Both strains exhibited similar flux of glucose consumption and ethanol synthesis but important differences in carbon distribution with biomass/substrate yields and ATP production 50% higher in *P-*. A higher contribution of fermentative metabolism, with 64% of the energy produced at the phosphorylation level, was observed during SOD production. The flux of precursors to amino acids and nucleotides was higher in the recombinant strain, in agreement with the higher total RNA and protein levels. Lower specific growth rates in strain *P+* appear to be related to the decrease in the rate of synthesis of nonrecombinant protein, as well as a decrease in the activities of the pentose phosphate (PP) pathway and TCA cycle. A very different way of entry into the stationary phase was observed for each strain: in the wild-type strain most metabolic fluxes decreased and fluxes related to energy reserve synthesis increased, while in the *P+* strain the flux of 22 reactions (including PP pathway and amino acids biosynthesis) related to SOD production increased their fluxes. Changes in SOD production rates at different

physiological states appear to be related to the differences in building blocks availability between respirofermentative and oxidative metabolism. Using the present expression system, ideal conditions for SOD synthesis are represented by either active growth during respirofermentative metabolism or transition from a growing to a nongrowing state. An increase in SOD flux could be achieved using an expression system nonassociated to growth and potentially eliminating part of the metabolic burden. © 2003 Wiley Periodicals, Inc. *Biotechnol Bioeng* 82: 152–169, 2003.

Keywords: metabolic flux analysis; *S. cerevisiae*; recombinant protein; human SOD

INTRODUCTION

Saccharomyces cerevisiae is an attractive host for the production of heterologous proteins since it can perform post-translational processing and modifications of many mammalian proteins. Therefore, the synthesis of recombinant protein in *S. cerevisiae* has become an important issue for commercial production of recombinant proteins and hence an interesting subject for metabolic engineering. Metabolic flux analysis (MFA), as one of the essential tools for pathway analysis and modification (Stephanopoulos et al., 1998), could be of great value in studying this system.

During batch growth in glucose-limited cultures, *S. cerevisiae* will display both respiratory (purely oxidative) metabolism or respirofermentative (oxidative/reductive) metabolism. This behavior is known as diauxic growth. The growth begins with a respirofermentative phase where cells grow at their maximum specific growth rate, the glucose uptake rate exceeds the capacity for total oxidation, and part of it is converted to ethanol and other fermentation products. When glucose is exhausted, the produced ethanol is used as an energy and carbon source and the culture enters the respiratory phase. The respirofermentative characteristics depend on the strain and environmental conditions (Cortassa and Aon, 1994, 1997).

*Present address: Department of Chemical Engineering, Iowa State University, Ames, Iowa 50011-2230.

Correspondence to: Juan A. Asenjo

Contract grant sponsor: Conicyt

Contract grant number: Fondecyt 2990095

Contract grant sponsor: the Millennium Institutes Programme

Contract grant number: P 99031-F

The expression of recombinant genes has an effect in the host organism known as the biosynthetic burden (Bentley et al., 1990; Janes et al., 1990; Snoep et al., 1995; Martinez et al., 1999), which negatively affects cell growth. Several explanations have been proposed for such a metabolic burden (Carlsen et al., 1997; Ibba et al., 1993; Lang and Looman, 1995; Lopes et al., 1996; Martinez et al., 1999), including 1) the allocation of cellular resources in replication and maintenance of the expression system, transcription of the recombinant gene, and synthesis of the recombinant protein; 2) the dilution of nonrecombinant protein; 3) the effect of foreign DNA synthesis during plasmid replication; and 4) the toxicity of the recombinant protein being produced. Recently, Gorgens et al. (2001) studied the effect of each component of the expression system on the metabolic burden that recombinant protein synthesis imposes on *S. cerevisiae*.

Even when several studies exist in this area, no previous analysis has been done using MFA that allows the quantification and study of metabolic fluxes in the presence and absence of recombinant protein synthesis and the relation of oxidative/reductive metabolism with recombinant protein synthesis. In this context, the objective of this work is to study the synthesis of high levels of intracellular recombinant protein (human superoxide dismutase, SOD) in *S. cerevisiae* rhSOD 2060 411 SGA122 cultures and its comparison with the wild-type strain (without the expression system, not producing the recombinant protein). SOD catalyzes the destruction of the O_2^- free radical. It protects oxygen-metabolizing cells against harmful effects of superoxide free radicals. Human SOD consists of two subunits of identical molecular weight joined by a disulfide bond. The molecular weight is 32,500 (Keele et al., 1971). There are two Cu(II) and two Zn(II) atoms per molecule (Bannister et al., 1971). SOD has been shown to exert strong regenerative effects on tissues that have become hardened or fibrotic because of age, disease, or injury (Lefaix, 1993). SOD therapy has been used successfully to treat fibrotic scarring of organs after radiation therapy, to prevent further heart damage in cardiac patients, and to improve severe rheumatoid arthritis.

MATERIALS AND METHODS

Strains and Medium

Recombinant *S. cerevisiae* rhSOD 2060 411 SGA122 (MAT α , *leu2*) was kindly provided by Chiron Corp. (Emeryville, CA). This strain harbors the plasmid pC1/1PGAPSOD (promoter and terminator from the enzyme glyceraldehyde phosphate dehydrogenase (GAP), and leucine marker) allowing the synthesis of high levels of human SOD (Hallewell et al., 1987; Hallewell and Mullenbach, 1998). The SOD gene is constitutively expressed from a GAP promoter. A second strain derived from *S. cerevisiae* rhSOD 2060 411 SGA122 was also used, which contains no

expression vector, does not produce SOD, and exhibits a leucine auxotrophy. The strain containing the expression system (recombinant strain in this study) was designated as *P+*, and the strain not containing the expression system (wild type) as *P-*. Strains were maintained on plates with complex medium (see below) and 1.5% of agar. Two culture mediums were used: 1) mineral salt medium (Verduyn et al., 1990), and 2) complex medium. The complex medium contained (per liter): 10 g of yeast extract, 20 g of peptone, and 0.5 g of $CuSO_4 \cdot 5H_2O$. The mineral salt medium contained (per liter): 10.0 g of glucose, 5.87 g of $(NH_4)_2SO_4$, 1.17 g of KH_2PO_4 , 0.43 g of $MgSO_4 \cdot 7H_2O$, 4 ml of trace metal solution, 10.0 ml of $CuSO_4 \cdot 5H_2O$ solution, and 2 ml of vitamins solution. Copper sulfate and vitamins solution were sterilized by filtration; 100 mM citrate buffer was used to keep the pH at a value of 5. Trace metals solution contained (per liter): 1.0 g of $FeSO_4 \cdot 7H_2O$, 1.5 g of $ZnSO_4 \cdot 7H_2O$, 1.5 g of $CaCl_2$, 0.32 g of $MnCl_2 \cdot 2H_2O$, 0.30 g of H_3BO_3 , 0.10 g of $CoCl_2 \cdot 6H_2O$, 0.10 g of MoO_3 , and 0.03 g of KI. Mineral salt medium was supplemented with 0.7 g/L of leucine. The vitamin solution contained (per liter): 0.04 g of biotin, 0.67 g of pantothenate, 0.67 g of nicotinamide, 8.3 g of inositol, 0.67 g of thiamin-HCl, 0.67 g of pyridoxine-HCl, and 0.1335 g of p-aminobenzoic acid. Copper sulfate solution contained 100 g/L of $CuSO_4 \cdot 5H_2O$. During *P-* strain cultures copper concentration was 10^{-3} g/L.

Fermentations

Fermentations were carried out in a fully equipped fermentor (Biostat B; B. Braun Biotech International, Germany) with a working volume of 1 L. The bioreactor was operated in batch mode at 30°C, pH 5 (citrate buffer), airflow of 2 L/min, and 600 rpm. Under these conditions, dissolved oxygen was always above 60% of the saturation levels, ensuring no oxygen limitation. The fermentor was equipped with a chilled water condenser that prevents ethanol loss by evaporation. The inoculum was prepared by initially transferring three fresh colonies from solid medium into a 125 ml flask containing 25 ml of complex medium. Flasks were incubated for 12–14 h (*P-* and *P+* strain, respectively), and the culture was harvested using the pellet in the inoculation of a 500 ml flask containing 150 ml of mineral salt medium supplemented with leucine (and copper, when *P+* strain was used). The pellet obtained from the last culture during exponential growth on glucose was used as inoculum for experiments in the fermentor.

Analytical Procedures

Twenty to 50 ml samples (depending on the culture time) were removed from the fermentor for the measurement of cell mass, total RNA, total protein, total carbohydrates, glucose, ethanol, and human SOD. All measurements were performed in triplicate and the results are presented as average and standard deviations. Samples were kept in an

ice-water bath, aliquotted into small volumes, and centrifuged at 15,000 rpm for 5 min in an Eppendorf 5403 centrifuge at 0°C. Supernatant was stored at -20°C for glucose, ethanol, and glycerol analysis. Pellets, after washing twice with cold 9 g/L NaCl, were stored at -80°C for total RNA, total protein, total carbohydrates, and SOD analysis. Total RNA was extracted with perchloric acid (after eliminating free sugars) and quantified using orcinol as suggested by Herbert et al. (1971). Total protein was extracted with hot NaOH and quantified with Folin-Ciocalteu reagent (Lowry's method; Peterson, 1977). Total carbohydrates were measured using the anthrone method (Herbert et al., 1971). SOD measurement involved cell disruption (1 OD (600 nm) pellet resuspended in lysis buffer) by three cycles of freezing (-80°C) and thawing in a boiling water bath (Sambrook et al., 1989). The cell extract was subjected to polyacrylamide gel electrophoresis (SDS-PAGE, 12%), where molecular weight markers and SOD standards were included. SOD spots were quantified using SigmaGel (Jandel Scientific Co., Sausalito, CA) software. Cell concentration was measured as dry weight using 2–3 ml of culture, filtered through a 0.47 µm filter paper, and dried at 110°C for 24 h. Total lipids were calculated using total RNA, total protein, total carbohydrates, SOD, and cell concentration measurements, and considering a 3% ash content (Nielsen and Villadsen, 1994). Glucose and ethanol concentration were measured enzymatically using Sigma kits (procedure number 510 and 332-UV, respectively; Sigma Diagnostics, St. Louis, MO). Oxygen consumption rate was measured monitoring the variation of dissolved oxygen (DO) concentration after cutting off the air supplied to the fermentor. Plotting DO vs. time, a straight line is obtained and its slope represents the volumetric oxygen consumption rate.

Stoichiometric Model and Flux Calculation

Metabolite balancing has been extensively used for the quantification of metabolic fluxes in cells grown under balanced conditions: i.e., exponential growth in batch cultures and steady-state chemostats (Stephanopoulos et al., 1998). Using this methodology, the intracellular fluxes can be calculated from a few measured fluxes by using mass balances for the intracellular metabolites, which are considered in steady state. The two determinants in this process are: 1) the stoichiometric model, and 2) the measured fluxes. A stoichiometric model was built considering the most important pathways operative under the conditions studied and is shown in Appendix A. The model resembles previous stoichiometric models (Vanrolleghem et al., 1996; Nissen et al., 1997; Ostergaard et al., 2001), its main features being: i) inclusion of respirofermentative metabolism with the production of ethanol and glycerol under aerobic conditions (the singularity introduced by considering the production of ethanol from pyruvate (Vanrolleghem et al., 1996) is avoided by the compartmentalization of acetyl-coenzyme A; see Appendix A); ii) synthesis of recombinant protein (SOD) from individual amino acids; iii) a pooled equation

for ATP consumption in maintenance, futile cycles, transport, and protein processing; and iv) the P/O ratio was 1.09 moles ATP/mol O₂ (Vanrolleghem et al., 1996). The model includes 78 reactions (fluxes), three of which are not considered (reactions 12, 29, and 52), reducing the number of fluxes to 75. In all, 63 out of the 80 metabolites included in the model could be considered in steady state without introducing singularities, resulting in a system with 12 degrees of freedom. Two versions of the stoichiometric model were used: one for cell growth on glucose (Glucose Model) and the other one for cell growth on ethanol/glycerol (Ethanol Model). In the Glucose Model the following assumptions were made: a) reactions specific to gluconeogenesis (reactions 4 and 8) were considered either not to be active or introducing futile cycles already included in equation 69; b) the glyoxylate cycle was considered inactive (de Jong-Gubbels et al., 1995); and c) all AcCoA entering the TCA cycle was considered to be produced by the enzyme pyruvate dehydrogenase, and no transport of AcCoA from the cytoplasm to the mitochondria takes place (Nissen et al., 1997; Ostergaard et al., 2001). This assumption reduces the degrees of freedom to 8, equaling the number of measured fluxes under these conditions (glucose, ethanol, carbohydrates, lipids, total protein, total RNA, SOD, and O₂), and resulting in a determined system. In the Ethanol Model the following assumptions were made: I) the glucose consumption reaction (Eq. 3, Appendix A) was not included, irreversible glycolytic steps were considered inactive (Eqs. 3, 9, Appendix A); II) Eq. 26, representing the pyruvate overflow mechanism, was not included; and III) conversion of pyruvate to oxaloacetate (Eq. 23, Appendix A) was not included to avoid a futile cycle already considered in Eq. 69. The above assumptions reduce the degrees of freedom to 7, which equals the number of measured fluxes (ethanol, carbohydrates, lipids, total protein, total RNA, SOD, and O₂), and results in a determined system. The whole set of equations for the stoichiometric model, as well as a summary of the Glucose and Ethanol Models, can be found in Appendix A. Using stoichiometric models and measured fluxes, all considered metabolic fluxes are calculated and the metabolic differences between cells, producing and not producing high levels of SOD, can be identified and related to differences in fermentation behavior. This kind of phenotypic evaluation through metabolic fluxes quantification also allows the quantification of the so-called "metabolic burden" imposed by SOD production (introduction of an expression system and synthesis of SOD) and to identify ideal conditions for its synthesis.

RESULTS AND DISCUSSION

Aerobic Growth of *Saccharomyces cerevisiae* rhSOD 2060 411 SGA122 Strain (P+) and Its Wild Type (P-) in Glucose-Limited Batch Cultures.

Strains *S. cerevisiae* rhSOD 2060 411 SGA122 (P+, i.e., with expression system and producing SOD) and its wild

type (*P*−, i.e., without expression system and not producing SOD) were initially grown in batch cultures using complex medium (data not shown), obtaining almost identical fermentation profiles. Specific growth rates during growth on glucose were 0.45 h^{−1} and 0.46 h^{−1} for *P*− and *P*+, respectively, while specific growth rates on ethanol were 0.084 h^{−1} and 0.076 h^{−1} for *P*− and *P*+, respectively. This result could suggest that no additional metabolic resources for replication and maintenance of the plasmid were needed (Gorgens et al., 2001) when growing on glucose. Therefore, comparison of these strains during growth on mineral salt medium will probably quantify how transcription of recombinant genes and synthesis of recombinant proteins affect the metabolic activity of the cells. Considering the high levels of SOD produced by strain *P*+, (up to 30% of total protein, see below), transcription of the gene encoding SOD and its synthesis will probably be the major contribution to the observed metabolic burden. Ultimately, this type of study evaluates the metabolic effect resulting from the production of high levels of intracellular SOD, including the effect of introducing the expression system with all its components and its further replication, transcription, and translation.

Strains *P*+, and *P*− were grown on minimum salts medium in batch culture. Figure 1A,B shows the time profiles of cell growth and SOD production, as well as glucose and ethanol concentration in the medium. Both strains exhibited diauxic growth, with a first phase of growth on glucose and a second phase on ethanol. Respirofermentative metabolism during growth on glucose results in the production of fermentation products that are consumed after glucose is exhausted from the medium in a second growth phase. Only the amounts of ethanol and glycerol produced are important—others, such as succinate or acetate, account for less than 1% of sugar consumed (Gancedo and Serrano, 1989). Ethanol was measured and glycerol, even though not measured, was included in the model. The above-described profile is similar for both strains, as is the amount of ethanol produced and the time at which a switch between respirofermentative and oxidative metabolism takes place. However, maximum cell concentration at stationary phase was 41% higher in strain *P*−. Figure 1A also includes the time profile for human SOD synthesis. SOD is synthesized mainly during exponential growth on glucose and at the entry into the stationary phase, where it represented about

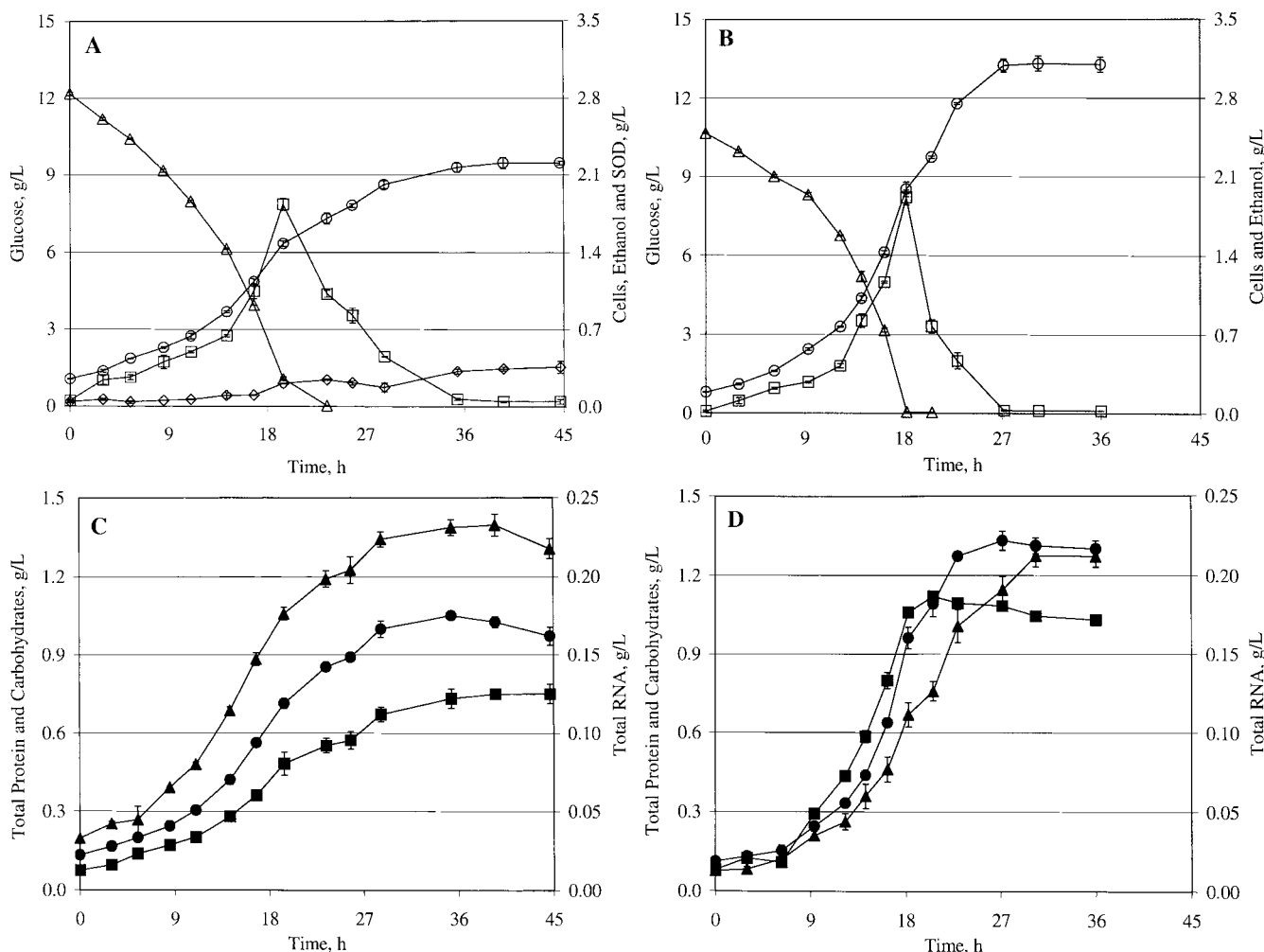


Figure 1. Growth of *S. cerevisiae* rhSOD 2060 411 SGA122 (A,C) and its wild type (B,D) in glucose-limited batch cultures. Symbols represent the concentration (g/L) of: (Δ) glucose, (□) ethanol, (○) cells, (◇) SOD, (▲) total RNA, (●) total protein, and (■) total carbohydrates.

30% of total cell protein. However, its levels remain constant during exponential growth on ethanol. This profile is different from those found during the synthesis of other recombinant protein in *S. cerevisiae* where *PGK1* and *ADH2* promoters were used (Cartwright et al., 1994; Dickson and Brown, 1998; Gorgens et al., 2001), and recombinant proteins were produced during growth on ethanol. The expression system used in this work contains the *GAP* promoter, allowing the constitutive expression of the gene codifying for SOD (Hallewell and Mullenbach, 1998). It means the absence of SOD synthesis during growth on ethanol, and in fact during oxidative metabolism, which is not due to a promoter-related problem.

In the above experiments, exponential growth on glucose and ethanol was verified (Appendix B). Biomass/substrate (biomass/glucose and biomass/ethanol) and product/substrate (ethanol/glucose) yields were calculated during exponential growth phases for both strains, shown in Table I. Ethanol/glucose yields were similar in both strains, but biomass/glucose and biomass/ethanol yields were 49 and 38% higher in strain *P*–. These results show a decreased efficiency of the *P*+ strain to convert substrates (glucose and ethanol) into cellular components. This behavior is presumed to be related to SOD synthesis and has been reported for other *S. cerevisiae* strains producing recombinant proteins (Gorgens et al., 2001). However, the magnitude of the differences in our system is larger than in the previous report (for example, the 50% difference in biomass/glucose yield found in this work compared to the 13% found in Gorgens et al., 2001). The larger differences are probably related to the high levels of SOD produced by the *P*+ strain. Higher biomass/substrates yields in *P*– are in agreement with the higher cell concentration in this strain, while similar ethanol/glucose yields agree with equal ethanol concentration in both cultures.

Figure 1C,D shows the time profile for the concentration of measured cellular components in both strains: i.e., total protein, total carbohydrates, and total RNA. Profiles are similar to those observed for cell concentration in each strain. The only difference between the two strains was the change in total RNA concentration during late exponential growth on ethanol and entry into stationary phase. During this period, total RNA was maintained at constant levels in strain *P*–, while in strain *P*+ an increase was observed. This behavior could be related to the resumption of SOD pro-

duction by *P*+ during late exponential growth on ethanol and entry into the stationary phase. The above measurements, along with cell concentration measurements, were used to calculate the distribution of different cell fractions in the dry weight of strains *P*+ and *P*– (assuming 3% of ash). Approximately constant values were obtained for both exponential growth phases; average values and standard deviation for growth on glucose are shown in Table II. A Student's *t*-test was used to compare cell fractions between the different strains, resulting in significant differences in all cases (see *P*-value in Table II). Strain *P*+ increased total protein and total RNA levels in comparison to wild-type strain *P*–. This increment accounts for a decrease in total carbohydrates and total lipids fractions in *P*+.

Specific Rates

The differences between strains *P*+ and *P*– include fermentation profiles and yields and also specific rates. Using cell concentration measurements, specific rates for both strains during exponential growth on glucose and ethanol were calculated and are shown in Table I. Strain *P*– exhibited a higher specific growth rate than *P*+ in both phases of growth (on glucose a 1.52-fold increase and on ethanol a 2.13-fold increase). Similar results have been reported for other *S. cerevisiae* strains producing recombinant proteins (Da Silva and Bailey, 1991; Dequin and Barre, 1994; Gorgens et al., 2001) but the differences observed in our system are larger than previously reported. This could also be related to the high levels of intracellular SOD produced in this strain. Measurements of total RNA, total carbohydrates, total protein, and SOD, as well as glucose and ethanol concentration in the medium, were used to calculate corresponding specific rates. Estimated total lipid concentration was also included in this calculation; the results are shown in Tables III and IV. Specific rates during three phases are included: 1) exponential growth on glucose, 2) exponential growth on ethanol, and 3) entry into the stationary phase. Negative and positive values mean consumption or production, respectively. Specific details of the calculations are given in Appendix B. Note that even when total protein and total RNA fractions are higher in strain *P*+, the specific rates at which these cellular fractions are produced are

Table I. Yields, specific growth rate, and energy production in recombinant (*P*+) and wild-type (*P*–) strains.

Strain	Yield (g/g)			Specific growth rate		ATP production during growth on glucose		
	Biomass glucose	Biomass ethanol	Ethanol glucose	Glucose (h ⁻¹)	Ethanol (h ⁻¹)	Flux*	Yield mol ATP mol gluc.	Respiratory chain (%)
<i>P</i> +	0.111	0.385	0.161	0.1042	0.0698	21.50	4.66	36.09
<i>P</i> –	0.165	0.530	0.153	0.1586	0.0327	33.45	6.92	47.86
<i>P</i> –/ <i>P</i> +	1.49	1.38	0.95	1.52	2.13	1.56	1.48	1.33

*Expressed in mmoles ATP/(g Cell·h).

Table II. Comparison of macromolecular composition (%) of wild-type (*P*−) and recombinant strain (*P*+) .

Component	Strain <i>P</i> +	Strain <i>P</i> −	<i>P</i> -value
Protein	49.23 ± 0.68	45.69 ± 2.30	0.005
Carbohydrates	32.37 ± 0.69	34.28 ± 1.51	0.018
RNA	11.96 ± 1.00	8.70 ± 1.12	0.000
Lipids	3.44 ± 1.40	8.34 ± 1.70	0.000

higher in strain *P*−. This means that specific rates of synthesis of all cellular fractions are higher in strain *P*− during exponential growth on glucose and ethanol.

Distribution of Metabolic Fluxes in Recombinant (*P*+) and Wild-Type (*P*−) Strain

The analysis of metabolic flux distribution in strains *P*+ and *P*− was carried out using two versions of the proposed stoichiometric model: 1) the glucose model, and 2) the ethanol model. Using these models and measured fluxes (Tables III, IV), all metabolic fluxes considered in the model were calculated. Figure 2 shows the distribution of metabolic fluxes of central metabolic pathways in the recombinant strain. Flux values for exponential growth on glucose, exponential growth on ethanol, and entry into stationary phase are included in this figure. To facilitate the comparison between the two strains, metabolic flux distribution for wild-type strain (*P*−) is presented in Figure 3.

During exponential growth on glucose under aerobic conditions both strains consume glucose and produce fermentation products (ethanol and glycerol). There is no operation of the glyoxylate cycle, and the only operative anaplerotic reaction is the conversion of pyruvate to oxaloacetate by the enzyme pyruvate carboxykinase (Figs. 2, 3).

In the second exponential phase of growth (on ethanol), the consumed ethanol supported growth of the *P*+ strain. In

Table III. Specific rates (mmol/(g Cell · h)) calculated from measured compounds in recombinant strain (*P*+) during growth on minimum salts medium.

Phase compound	Growth on glucose exponential	Growth on ethanol		Molecular weight, g/mol
		Exponential	Entry stationary phase	
Glucose	−4.611			180.0
Ethanol	4.130	−1.826	−0.598	46.0
Protein ^a	0.351	0.144	0.033	111.4
SOD ^b	0.109	0.000	0.137	109.4
RNA ^a	0.042	0.012	0.002	318.3
Lipids ^{a,c}	0.005	0.002	0.004	655.0
Carbohydrates ^a	0.208	0.065	0.027	162.0
Oxygen	−3.564	−3.461	−3.399	32.0

^aExpressed as total levels in the cell.
^bSuperoxide dismutase.
^cCalculated using the measurements of dry weight and considering 3% of ash.

Table IV. Specific rates (mmol/(g Cell · h)) calculated from measured compounds in wild-type strain (*P*−) during growth on minimum salts medium.

Phase compound	Growth on glucose exponential	Growth on ethanol		Molecular weight, g/mol
		Exponential	Entry stationary phase	
Glucose	−4.833			180.0
Ethanol	4.130	−2.174	−0.772	46.0
Protein ^a	0.640	0.302	0.042	111.4
SOD ^b	0.000	0.000	0.000	109.4
RNA ^a	0.046	0.019	0.000	318.3
Lipids ^{a,c}	0.021	0.007	0.016	655.0
Carbohydrates ^a	0.332	0.014	0.069	162.0
Oxygen	−7.365	−5.882	−5.383	32.0

^aExpressed as total levels in the cell.
^bSuperoxide dismutase.
^cCalculated using the measurements of dry weight and considering 3% of ash.

the case of *P*−, ethanol and glycerol were consumed to support growth. The absence of glucose in the medium and the use of ethanol as the carbon source results in the activation of the glyoxylate cycle and the enzyme phosphoenolpyruvate carboxykinase (conversion of oxaloacetate to pyruvate), and reverse operation of some glycolytic steps (gluconeogenic pathway instead of glycolysis). Other reactions specific to ethanol consumption increase their flux compared to exponential growth on glucose. They include the conversion of acetaldehyde to acetate (acetaldehyde dehydrogenase), the production of cytoplasmic AcCoA from acetate (AcCoA synthase), and the transport of AcCoA from cytoplasm to mitochondria (Figs. 2, 3). The transition from exponential growth on glucose to exponential growth on ethanol was accompanied by a decrease of almost all metabolic fluxes due to lower metabolic activities: lower specific growth rates and lower substrate consumption and product synthesis.

No SOD was produced during exponential growth on ethanol resulting in higher differences between the two strains in the use of amino acids for nonrecombinant protein synthesis (Figs. 2, 3): 2.1-fold higher in *P*−, in agreement with a 2.1-fold increase of specific growth rate in *P*− during this phase. SOD was only produced during exponential growth on glucose and during entry into the stationary phase. Therefore, the metabolism of strains *P*+ and *P*− during these phases will be compared.

Differences in Metabolic Flux Distribution between Recombinant (*P*+) and Wild-Type (*P*−) Strain: Exponential Growth on Glucose

A more detailed analysis of Figures 2 and 3 reveals a similarity in the use of glucose and production of ethanol by both strains during growth on glucose, behavior that differs from a previous report on the synthesis of recombinant pro-

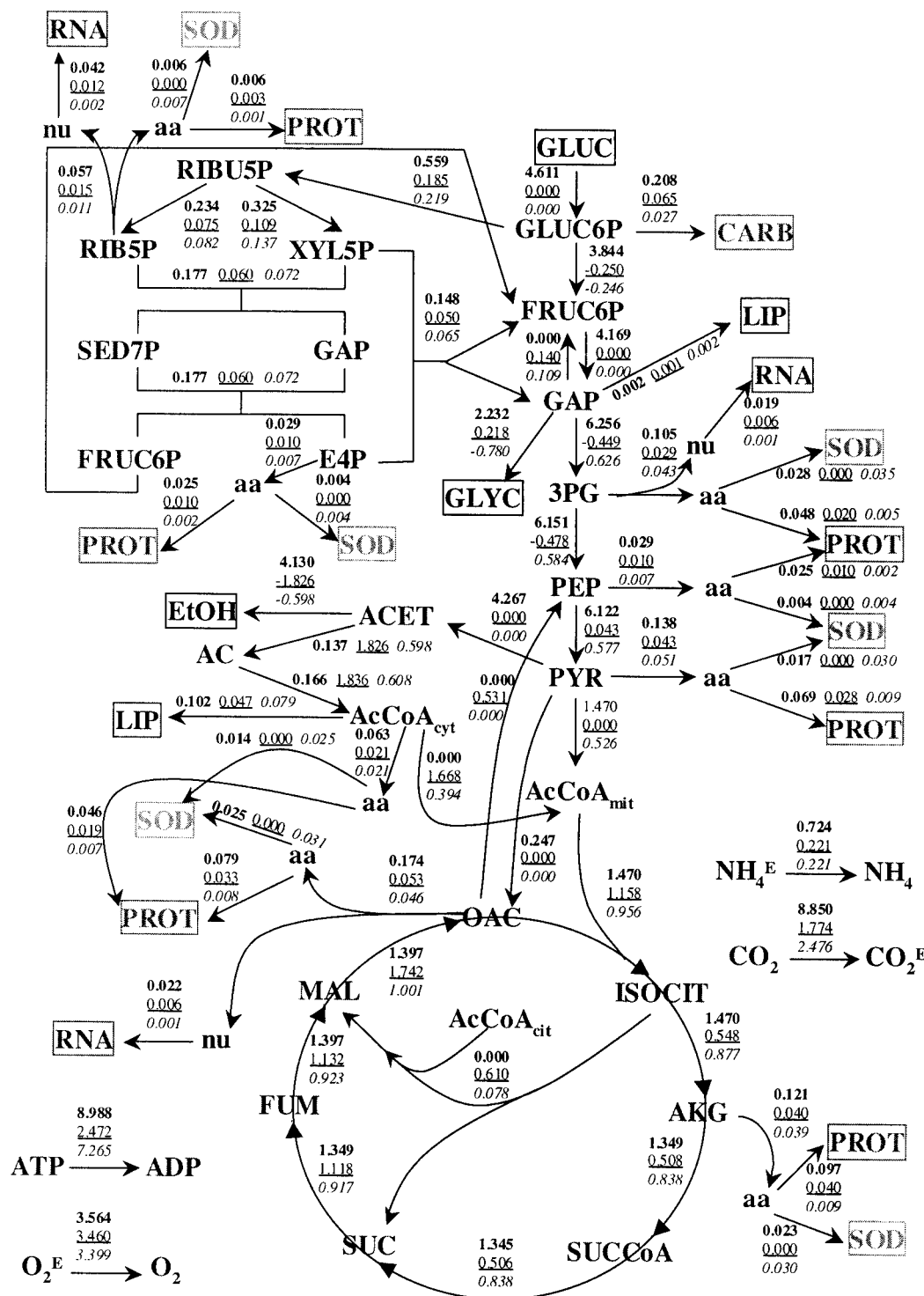


Figure 2. Distribution of metabolic fluxes in recombinant strain (*P+*) at different growth phases: 1) exponential growth on glucose (bold); 2) exponential growth on ethanol (underlined); and 3) entry into stationary phase (italics). Flux values are expressed in mmol/(g Cells.h). aa: amino acids, nu: nucleotides. See Appendix A for notation.

tein in other strains of *S. cerevisiae* (Gorgens et al., 2001). Despite these similarities, strain *P+* exhibited a stronger fermentative behavior, as can be seen by its higher glycerol synthesis flux and less active respiratory metabolism (lower TCA cycle). Figures 2 and 3 clearly show similar fluxes in both strains for half of the glycolytic steps (conversion of

glucose to glyceraldehydes phosphate), while the other half (conversion of glyceraldehyde phosphate to pyruvate) exhibited a flux 23% higher in *P-* strain. This result is in contrast to the approximately 60 and 80% increase in TCA cycle (oxidative metabolism) and PP pathway activities (supply of reducing power, NADPH) in the *P-* strain,

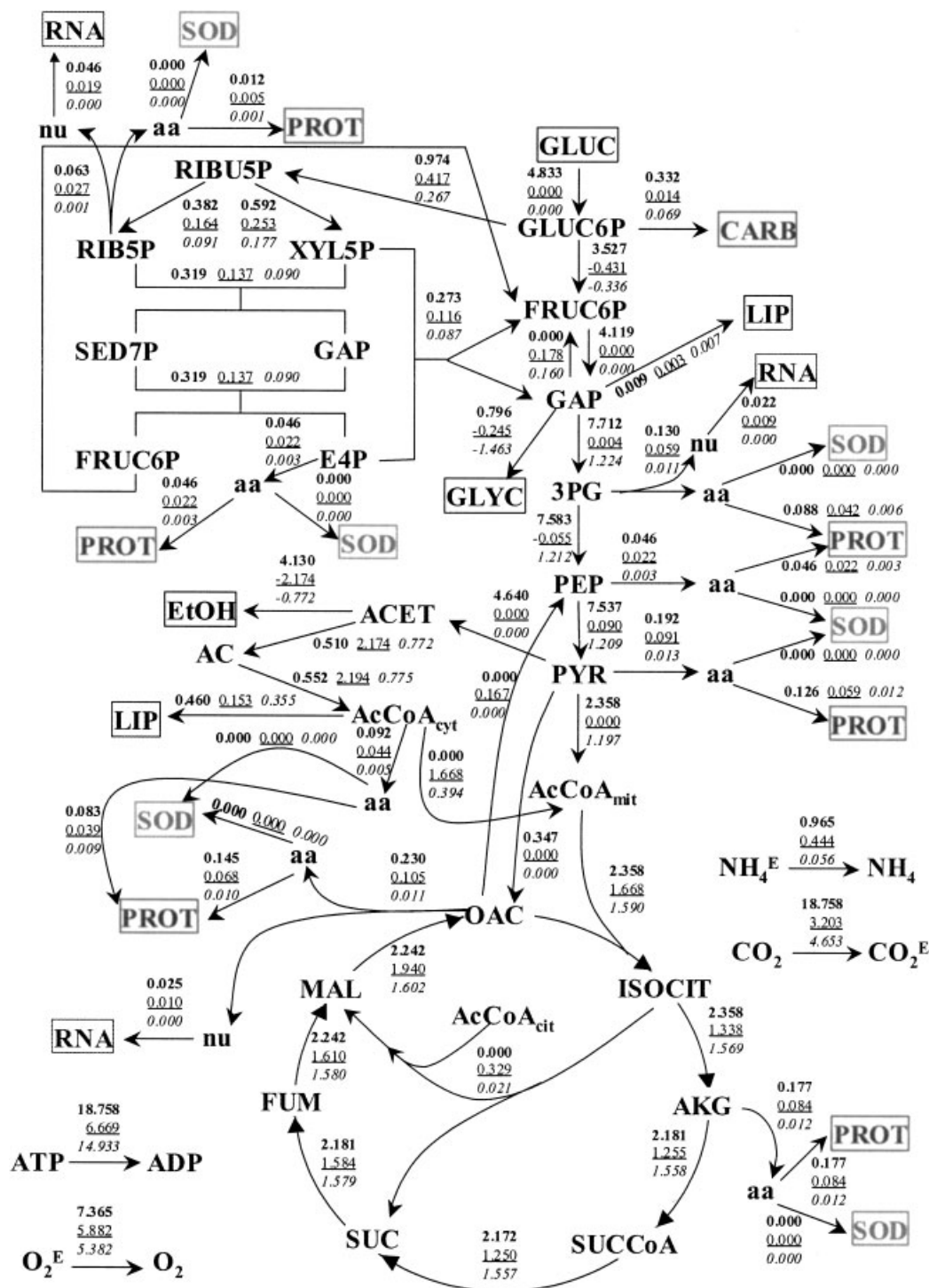


Figure 3. Distribution of metabolic fluxes in wild-type strain (*P*-) at different growth phases: 1) exponential growth on glucose (bold); 2) exponential growth on ethanol (underlined), and 3) entry into stationary phase (italics). Flux values are expressed in mmol/(g Cells.h). aa: amino acids, nu: nucleotides. See Appendix A for notation.

which could be responsible for higher specific growth rates of this strain. The relative contribution of oxidative and fermentative metabolism in Crabtree-positive strains is currently under debate (Van Hoek et al., 1998). In this study, strain *P*- appears to be able to increase the contribution of oxidative metabolism to fulfill the higher requirements of energy and precursors allowing the increase in specific

growth rate. In strains *P*- and *P*+, rate-limiting steps of the respiratory pathways appear to be located in steps after the synthesis of pyruvate and not related to the enzyme pyruvate decarboxylase: the flux through this step (conversion of pyruvate to acetaldehyde) and the production of ethanol are not affected by the changes in oxidative/fermentative metabolism. Reactions involved in the synthesis of cytoplas-

mic AcCoA and lipid synthesis also increased their fluxes (3.5- and 4.5-fold, respectively) in strain *P*–.

Fluxes of building blocks synthesis and their consumption in the production of macromolecules were also higher in strain *P*–, and this is directly related to the higher specific growth rate of this strain. The observed increase in metabolic fluxes in the *P*– strain could be related to an increase in either specific activity of the enzyme catalyzing each

reaction or an increase in their levels. The observed increase of more than 80% in the consumption of amino acids for nonrecombinant protein synthesis in strain *P*– (Figs. 2, 3) appears to be responsible for the increment in metabolic fluxes in this strain. In other words, the inclusion of the expression system and the synthesis of SOD result in a dilution of nonrecombinant proteins, including enzymes, causing the observed decrease in most metabolic fluxes in

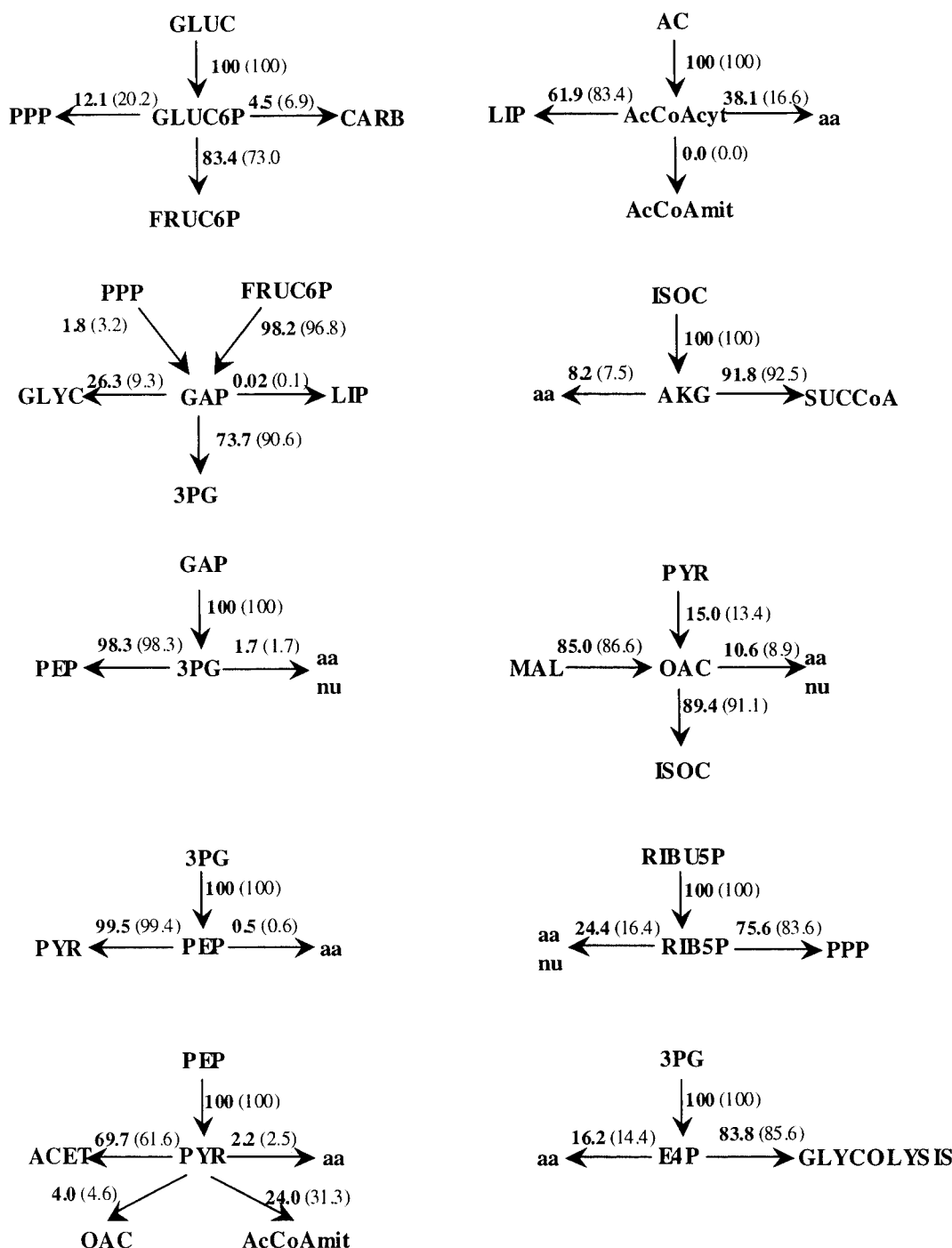


Figure 4. Flux partitioning (expressed as percent) at precursor metabolites during exponential growth on glucose. Values for recombinant strain (*P*+) are represented in bold and values in parenthesis were calculated for wild-type strain (*P*–). aa: amino acids, nu: nucleotides, LIP: lipids. See Appendix A for notation.

the recombinant strain (*P+*). Flux of ATP consumption for transport and maintenance increased in strain *P-*, in agreement with the higher specific rates of this strain (Nielsen and Villadsen, 1994).

The estimated fluxes were also used to calculate the rate of ATP synthesis, ATP yield, and the relative contributions of respiratory chain and substrate level phosphorylation to energy production. Table I summarizes the results obtained, which show a decrease in ATP synthesis rate, and ATP yield in the strain producing SOD (*P+*). Observed differences between *P+* and *P-* are similar to the differences in specific growth rate (approximately 50% higher in *P-*). The contribution of substrate level phosphorylation to energy production was more important in the *P+* strain, implying a higher contribution of fermentative metabolism.

The study of flux partition at key branch points is an important issue in metabolic flux analysis. Figure 4 shows partition of metabolic fluxes in both strains at the following branch points: glucose-6-phosphate (GLUC6P), glyceraldehyde phosphate (GAP), 3-phosphoglycerate (3PG), phosphoenolpyruvate (PEP), pyruvate (PYR), acetyl-coenzyme A (AcCoA), oxaloacetate (OAC), α -ketoglutarate (AKG), ribose-5-phosphate (RIB5P), and erythrose-4-phosphate (E4P). In all cases, with the exception of 3PG, the synthesis of SOD produces a variation in flux partition at branch points. The fraction of AcCoA_{cyt}, AKG, OAC, RIB5P, and E4P used in the synthesis of building blocks (amino acids and nucleotides) was increased with the synthesis of SOD. This is in agreement with the higher levels of total protein and total RNA in strain *P+* (Table II). There are only two branch points where the fraction used in the synthesis of amino acids is not affected by the synthesis of SOD: PEP and PYR. Note that branch points not affected by SOD production are located in the glycolytic pathway and those changing are intermediates of the TCA cycle and PP pathway. On the other hand, the fractions used in lipid and carbohydrate synthesis (GLUC6P, GAP, and AcCoA_{cyt} branch points) decrease during the synthesis of SOD (i.e., in *P+* strain), in agreement with the differences in cell composition between the two strains (Table II). In the glyceraldehyde phosphate branch point, the synthesis of SOD increased the fraction of GAP used in the synthesis of glycerol, decreasing the fraction going through the glycolytic pathway. Pyruvate was mainly consumed by the enzymes pyruvate decarboxylase (acetaldehyde synthesis) and pyruvate dehydrogenase complex (mitochondrial AcCoA synthesis). SOD synthesis increased the synthesis of acetaldehyde and decreased the production of mitochondrial AcCoA. Finally, a higher contribution of anaplerotic pathway (carboxylation of pyruvate by enzyme pyruvate carboxykinase) to the synthesis of oxaloacetate was observed in the strain producing SOD in comparison to *P-*. This is in agreement with the higher consumption of oxaloacetate and α -ketoglutarate for building blocks synthesis under these conditions and a higher need for replacement of TCA cycle intermediates.

Facing Stationary Phase: Comparison of Metabolic Flux Distribution in Strain P- Versus Strain P+

Comparison of flux distribution in each strain during transition from exponential growth on ethanol to stationary phase reveals important differences with respect to how each strain deals with entering the stationary phase. Strain *P-* does a "traditional" entry into the stationary phase with a decrease in most fluxes in agreement with the decrease in metabolic activity. On the other hand, strain *P+* exhibited an increase in most metabolic fluxes during this transition. Figure 5 shows calculated flux ratios ([entry into stationary phase]/[exponential growth on ethanol]) for each strain during their transition from exponential growth on ethanol to stationary phase.

There are some similarities in how the two strains face the stationary phase. Two groups of reactions exhibited an increase in metabolic fluxes in both strains: 1) reactions involved in the conversion of glyceraldehyde phosphate to pyruvate, and 2) the TCA cycle reaction converting isocitrate to succinate. In both cases these changes are related to the increase in glycerol consumption during transition from exponential growth on ethanol to stationary phase. A reasonable explanation for this behavior is the increase in specific glycerol consumption rate (and decrease in specific ethanol consumption rate), which makes glycerol the main provider of precursor metabolites in the glycolytic pathway, PP pathway, and TCA cycle. Under these conditions, an increase in the flux of steps converting glyceraldehyde-3-phosphate to pyruvate is reasonable. Furthermore, the decrease in ethanol consumption results in a lower activity of the glyoxylate cycle and more isocitrate will be converted to succinate (through α -ketoglutarate) by reactions specific to the TCA cycle. This explains the increase in the two groups of reactions named above. Two other reactions, involved in the synthesis of lipids, dramatically increased their fluxes (to levels similar to those observed during growth on glucose) in both strains during transition to the stationary phase. Probably, an increase in the lipid fraction is a common mechanism these strains use to build a more robust cell wall to deal with stress conditions imposed by the stationary phase.

There is a group of reactions (22 reactions) that exhibited higher fluxes during entry into the stationary phase in strain *P+* but not in *P-*. They include all steps in the PP pathway (an increase of about 20% in their fluxes), 12 reactions involved in amino acids biosynthesis, and reactions consuming 3-phosphoglycerate and pyruvate for amino acids biosynthesis. The increase in these fluxes appears to be related to the higher flux of SOD synthesis during entry into the stationary phase (higher than calculated during exponential growth on glucose). The higher amino acids and reducing power (increase in PP activity) synthesis rates allow for the synthesis of higher levels of SOD under these physiological conditions. On the contrary, strain *P-* showed a decrease in most of its fluxes, and higher carbohydrate synthesis fluxes increasing its energy reserve which will

phase, SOD-specific mRNA still maintains its translation rate and there is an excess of amino acids, allowing the synthesis of SOD.

Using the above statement as a hypothesis, we could explain the changes in specific rates of SOD synthesis during different physiological states (growth phases in this case). During exponential growth on glucose the respirofermentative behavior of recombinant strain (*P*+) leads to an uncoupling between the availability of building blocks and their use in macromolecular synthesis: there is an “excess” of building blocks synthesis that allows their use in the synthesis of SOD (all steps in SOD synthesis have a competing equivalent in the synthesis of nonrecombinant protein). However, during exponential growth on ethanol a purely oxidative metabolism takes place with no uncoupling between central and biosynthetic metabolism: there is no “excess” of building blocks that will allow the synthesis of SOD, and indeed, SOD is not produced. During entry into the stationary phase, another uncoupling will be taking place: cells are mainly using the carbon source for carbohydrate synthesis as an energy reserve. Again, amino acids and nucleotides could be in “excess” and SOD can be synthesized. Although MFA does not allow identification of a control structure like the one described above, the distribution of metabolic fluxes agrees with the above description and allows targeting of appropriate conditions for SOD synthesis: 1) respirofermentative metabolism or 2) a metabolic state where a switch between a growing and nongrowing condition is taking place (in this study, transition from exponential growth on ethanol to the stationary phase). These findings have very important practical implications related to the culture and expression systems used during the production of SOD in *S. cerevisiae* strains. When a culture system allowing the manipulation of specific growth rate is used, attention should be paid to an adequate control of specific growth rate, ensuring the existence of respirofermentative metabolism (for example, fed-batch or continuous culture). On the other hand, the use of an expression system with a controlled promoter that will allow expression of the gene encoding SOD during transition from exponential growth on ethanol to stationary phase in a batch culture will probably be the best option. The use of an expression system with nongrowth-associated promoters and which is active during entry into the stationary phase could eliminate part of the metabolic burden and improve the synthesis rate and/or yield of SOD.

CONCLUSIONS

The synthesis of SOD in *S. cerevisiae* rhSOD 2060 411 SGA122 was accompanied by a decrease in specific growth rate (respect to wild-type strain) of 34 and 53% during growth on glucose and ethanol, respectively. Cellular composition was also affected, the total protein and RNA levels being higher in the recombinant strain (*P*+), while total carbohydrate and lipid fractions were lower. A stoichiomet-

ric model was built according to metabolic pathways operative in these strains during respirofermentative and oxidative metabolism. It allowed calculation of the distribution of metabolic fluxes during diauxic growth on glucose and ethanol. Comparison of metabolic flux maps showed important similarities and differences between the two strains and the different growth phases.

Both strains exhibited almost identical fluxes of glucose consumption and ethanol production, but important differences in the distribution of carbon source and in the efficiency of its conversion to biomass. Biomass/substrate yields were 50% higher in wild-type strain (*P*-), but flux of glycerol production were 36% higher in wild-type strain. Both ATP synthesis flux and ATP/substrate yield were 50% higher in strain *P*-. During growth on glucose, the synthesis of SOD was accompanied by a higher contribution of fermentative metabolism, with 64% of the total energy produced at the substrate phosphorylation level.

An analysis of flux partition in precursor metabolites revealed an increase in the fraction used in amino acids and nucleotides synthesis in the recombinant strain, in agreement with its higher levels of total protein and RNA. Fractions used in carbohydrate and lipid synthesis were lower in the *P*+ strain, in agreement with the decrease in carbohydrates and lipids levels. Differences observed in specific growth rate between the two strains appear to be related to the lower flux of nonrecombinant protein synthesis (including enzymes) in strain *P*+, as well as the decrease in the activities of PP pathway and TCA cycle. The transition from respirofermentative metabolism to oxidative metabolism in both strains was accompanied by a decrease in almost all fluxes, the activation of glyoxylate cycle and enzyme phosphoenolpyruvate carboxykinase, and reverse operation of some glycolytic enzymes (gluconeogenic pathway) allowing cell growth on ethanol.

Transition from exponential growth on ethanol to the stationary phase was very different in each strain. Strain *P*- did a “traditional” entry into the stationary phase, decreasing most metabolic fluxes, and increasing the synthesis of carbohydrates (energy reserve). Strain *P*+ exhibited an increase in the flux of 22 reactions, including the PP pathway and most steps in amino acids biosynthesis. This behavior was related to an observed increase in SOD synthesis during entry into the stationary phase that could possibly be due to a higher availability of building blocks.

Taken together, these results suggest that, using the present expression system, conditions that favor the synthesis of SOD are: 1) active growth during respirofermentative metabolism, and 2) a metabolic state where a switch between a growing and nongrowing state is taking place. In addition, the use of an expression system allowing SOD expression during transition from exponential growth to stationary phase will avoid a fraction of the metabolic burden and will improve specific production of SOD.

REFERENCES

- Bannister J, Bannister W, Wood E. 1971. Bovine erythrocyte cupro-zinc protein. I. Isolation and general characterization. *Eur J Biochem* 18: 178.
- Bentley WE, Mirjalili N, Andersen DC, Davis RH, Kompala DS. 1990. Plasmid encoded protein: the principal factor in the metabolic burden associated with recombinant bacteria. *Biotechnol Bioeng* 35:668–681.
- Carlsen M, Jochumsen KV, Emborg C, Nielsen J. 1997. Modeling the growth and proteinase A production in a continuous cultures of recombinant *Saccharomyces cerevisiae*. *Biotechnol Bioeng* 55:447–454.
- Cartwright CP, Li Y, Zhu YS, Kang YS, Tipper DJ. 1994. Use of B-lactamase as a secreted reporter promoter function in yeast. *Yeast* 10:497–508.
- Cortassa S, Aon MA. 1994. Metabolic control analysis of glycolysis and branching to ethanol production in chemostat cultures of *Saccharomyces cerevisiae* under carbon, nitrogen, or phosphate limitations. *Enzyme Microb Technol* 16:761–770.
- Cortassa S, Aon MA. 1997. Distributed control of the glycolytic flux in wild-type cells and catabolite repression mutants of *Saccharomyces cerevisiae* growing in carbon-limited chemostat cultures. *Enzyme Microb Technol* 21:596–602.
- Da Silva NA, Bailey JE. 1991. Influence of plasmid origin and promoter strength in fermentations of recombinant yeast. *Biotechnol Bioeng* 37:318–324.
- de Jong-Gubbels P, Vanrolleghem P, Heijnen S, van Dijken JP, Pronk JT. 1995. Regulation of carbon metabolism in chemostat cultures of *Saccharomyces cerevisiae* grown on mixtures of glucose and ethanol. *Yeast* 11:407–418.
- Dequin S, Barre P. 1994. Mixed lactic acid-alcoholic fermentation by *Saccharomyces cerevisiae* expressing the *Lactobacillus casei* L(+)-LDH. *Bio/Technol* 12:173–177.
- Dickson LM, Brown AJP. 1998. mRNA translation in yeast during entry into stationary phase. *Mol Gen Genet* 259:282–293.
- Gancedo C, Serrano R. 1989. Energy-yielding metabolism. In: Rose AH, Harrison JS, editors. *The yeasts*, vol. 3. London and San Diego: Academic Press. p 205–259.
- Gorgens JF, van Zyl WH, Knoetze JH, Hahn-Hagerdal B. 2001. The metabolic burden of the *PGK1* and *ADH2* promoter systems for heterologous xylanase production by *Saccharomyces cerevisiae* in defined medium. *Biotechnol Bioeng* 73:238–245.
- Hallewell RA, Mullenbach GT. 1998. United States Patent 5710033. Chiron Corp., Emeryville, CA.
- Hallewell RA, Mills R, Tekamp-Olson P, Blacher R, Rosenberg S, Ötting F, Masiaz FR, Scandella CJ. 1987. Amino terminal acetylation of authentic human Cu-Zn superoxide dismutase produced in yeast. *Bio/Technology* 5:363–366.
- Herbert D, Phipps PJ, Strange RE. 1971. Chemical analysis of microbial cells. In: Norris JR, Ribbons DW, editors. *Methods in microbiology*, vol. 5B. London: Academic Press.
- Ibba M, Kuhla J, Smith A, Kuenzi M. 1993. Stable continuous expression of a heterologous protein in *Saccharomyces cerevisiae* without selection pressure. *Appl Microbiol Biotechnol* 39:526–531.
- Janes M, Meyhack B, Zimmerman W, Hinnen A. 1990. The influence of GAP promoter variants on hirudin production, average plasmid copy number and cell growth in *S. cerevisiae*. *Curr Genet* 18:97–103.
- Keele B, McCord J, Fridovich I. 1971. Further characterization of bovine superoxide dismutase and the isolation from bovine heart. *J Biol Chem* 246:2875.
- Lang C, Looman AC. 1995. Efficient expression and secretion of *Aspergillus niger* RH5344 polygalacturonase in *Saccharomyces cerevisiae*. *Appl Microbiol Biotechnol* 44:147–156.
- Lefaix JL, Delanian S, Leplat JJ, Tricaud Y, Martin M, Hoffschir D, Daburon F, Baillet F. 1993. Radiation-induced cutaneo-muscular fibrosis (III): major therapeutic efficacy of liposomal Cu/Zn superoxide dismutase. *Bull Cancer* 80:799–807.
- Lopes TS, Wijs IJ, Steenhauer SI, Verbakel J, Planta RJ. 1996. Factors affecting the mitotic stability of high-copy-number integration into ribosomal DNA of *Saccharomyces cerevisiae*. *Yeast* 12:467–477.
- Martinez A, York SW, Yomano LP, Pineda VL, Davis FC, Shelton JC, Ingram LO. 1999. Biosynthetic burden and plasmid burden limit expression of chromosomally integrated heterologous genes (*pdC*, *adhB*) in *Escherichia coli*. *Biotechnol Prog* 15:891–897.
- Nielsen J, Villadsen J. 1994. *Bioreaction engineering principles*. New York and London: Plenum Press. p 55–82.
- Nissen TL, Schulze U, Nielsen J, Villadsen J. 1997. Flux distributions in aerobic, glucose-limited continuous cultures of *Saccharomyces cerevisiae*. *Microbiology* 143:203–218.
- Ostergaard S, Olsson L, Nielsen J. 2001. In vivo dynamics of galactose metabolism in *Saccharomyces cerevisiae*: metabolic fluxes and metabolite levels. *Biotechnol Bioeng* 73:412–425.
- Panek AD. 1991. Storage carbohydrates. In: Rose AH, Harrison JS, editors. *The yeast*, vol. 1. London: Academic Press. p 655–678.
- Papoutsakis ET, Meyer CL. 1985. Equations and calculations of product yields and preferred pathways for butanediol and mixed acid fermentations. *Biotechnol Bioeng* 27:56–66.
- Peterson G. 1977. A simplification of the protein assay method of Lowry et al., which is more generally applicable. *Anal Biochem* 83:346–356.
- Reardon KF, Scheper TH, Bailey JE. 1987. Metabolic pathway rates and culture fluorescence in batch fermentations of *Clostridium acetobutylicum*. *Biotechnol Prog* 3:153–167.
- Sambrook J, Fritsch EF, Maniatis T. 1989. *Molecular cloning: a laboratory manual*. Cold Spring Harbor, NY: Cold Spring Harbor Laboratory Press.
- Snoep JL, Yomano LP, Westerhoff HV, Ingram LO. 1995. Protein burden in *Zymomonas mobilis*: negative flux and growth control due to overproduction of glycolytic enzymes. *Microbiology* 141:2329–2337.
- Sogin SJ, Saunders CA. 1980. Fluctuation in polyadenylate size and content in exponential and stationary-phase cells of *Saccharomyces cerevisiae*. *J Bacteriol* 144:74–81.
- Stephanopoulos GN, Aristidou AA, Nielsen J. 1998. *Metabolic engineering*. London: Academic Press.
- Van Hoek P, Flikweert MT, Van der Aardt QJ, De Steensma HY, Van Dijken JP, Pronk JT. 1998. Effects of pyruvate decarboxylase overproduction on flux distribution at the pyruvate branch point in *Saccharomyces cerevisiae*. *Appl Environ Microbiol* 64:2133–2140.
- Vanrolleghem PA, de Jong-Gubbels P, van Gulik WM, Pronk JT, van Dijken JP, Heijnen S. 1996. Validation of a metabolic network for *Saccharomyces cerevisiae* using mixed substrate studies. *Biotechnol Prog* 12:434–448.
- Verduyn C, Postma E, Scheffers WA, van Dijken JP. 1990. Physiology of *Saccharomyces cerevisiae* in anaerobic glucose-limited chemostat cultures. *J Gen Microbiol* 136:395–403.
- Werner-Washburne M, Braun E, Johnston GC, Singer RA. 1993. Stationary phase in the yeast *Saccharomyces cerevisiae*. *Microbiol Rev* 57: 383–401.

APPENDIX A

Stoichiometric Model

The set of reactions and metabolites included in the stoichiometric model are shown below (I.1). Reactions not considered in the model are represented by an @ in front. Steps catalyzed by isoenzymes introduce singularity problems, which can be avoided using biochemical information about the relative contribution of each enzyme under the conditions studied. As reported previously (Nissen et al., 1997; Vanrolleghem et al., 1996), only one reaction was considered in the following two steps: 1) conversion of isocitrate

Table V. Summary of the two versions of the stoichiometric model used: glucose model and ethanol model.

Metabolic state	Number of metabolites	Un-steady state metabolites	Introducing singularities	Considered reactions	Degrees of freedom	Measured metabolites
Glucose model (Respirofermentative metabolism)	80	11	6	71 (4, 8, 24, and 75 were not included)	8	8
Ethanol model (Oxidative metabolism)	79	10	6	70 (1, 3, 9, 25 and 26 were not included)	7	7

to α -ketoglutarate (reaction 11, enzyme isocitrate dehydrogenase using NADH as cofactor), and 2) conversion of acetaldehyde to acetate (reaction 28, enzyme aldehyde dehydrogenase using NADH as cofactor). These assumptions leave the PP pathway as the only source of NADPH for biosynthesis. Leucine was included in the culture medium, and thus reaction 52 was not included in the model. The present model assumes the reaction catalyzed by acetyl-coenzyme A synthase as the only source of cytoplasmic AcCoA (Nissen et al., 1997; Ostergaard et al., 2001). During growth on ethanol, AcCoA entering the TCA cycle is provided by the above reaction. An equation representing AcCoA transport from cytoplasm to mitochondria was included (reaction 75), and it is only active during growth on ethanol. Two versions of the model were used: the Glucose Model representing the growth on glucose (respirofermentative metabolism) and the Ethanol Model representing growth on ethanol (oxidative metabolism). Table V summarizes each version of this model, including number of metabolites and reactions, metabolites introducing singularity problems, metabolites in un-steady state, degrees of freedom, and measured fluxes.

A sensitivity analysis, as described by Stephanopoulos et al. (1998), provides information about the sensitivity of calculated fluxes with respect to perturbation on measured fluxes. Using this approach we found that calculated fluxes were more affected by measurements in total protein and total RNA content in the cells. The measurement of these components was quite precise, with relative standard deviations of 1.5–3% for total RNA and 1.5–2.5% for total protein. Fluxes more affected by variation in measurements were the ones representing the rates of reactions 69 and 31–33. The first two reactions represent energy consumption for maintenance, transport, and proteins processing (reaction 69) and production or consumption of glycerol (reaction 31), which close mass and energy balances, respectively. The other two reactions represent the oxidative phosphorylation process, in which the P/O ratio is introducing uncertainty.

1.1. Metabolic Pathways and Metabolites Included in the Model

Glycolysis and Gluconeogenesis

1. $\text{GLUC} + \text{ATP} \Rightarrow \text{GLUC6P} + \text{ADP}$
2. $\text{GLUC6P} \Leftrightarrow \text{FRUC6P}$

3. $\text{FRUC6P} + \text{ATP} \Rightarrow \text{2GAP} + \text{ADP}$
4. $\text{2GAP} \Rightarrow \text{FRUC6P}$
5. $\text{GAP} + \text{NAD} + \text{ADP} \Leftrightarrow \text{G3P} + \text{ATP} + \text{NADH}$
6. $\text{G3P} \Leftrightarrow \text{PEP}$
7. $\text{PEP} + \text{ADP} \Rightarrow \text{PYR} + \text{ATP}$
8. $\text{OAC} + \text{ATP} \Rightarrow \text{PEP} + \text{ADP} + \text{CO}_2$

Tricarboxylic Acid (TCA) Cycle

9. $\text{PYR} + \text{NAD} \Rightarrow \text{AcCoA}_{\text{mit}} + \text{NADH} + \text{CO}_2$
10. $\text{AcCoA}_{\text{mit}} + \text{OAC} \Rightarrow \text{ISOCIT} + \text{CoA}$
11. $\text{ISOCIT} + \text{NAD} \Rightarrow \text{AKG} + \text{NADH} + \text{CO}_2$
12. $\text{@ISOCIT} + \text{NADP} \Rightarrow \text{AKG} + \text{NADPH} + \text{CO}_2$
13. $\text{AKG} + \text{CoA} + \text{NAD} \Rightarrow \text{SUCCoA} + \text{NADH} + \text{CO}_2$
14. $\text{SUCCoA} + \text{ADP} \Rightarrow \text{SUC} + \text{ATP} + \text{CoA}$
15. $\text{SUC} + \text{FAD} \Leftrightarrow \text{FUM} + \text{FADH}_2$
16. $\text{FUM} + \text{H}_2\text{O} \Leftrightarrow \text{MAL}$
17. $\text{MAL} + \text{NAD} \Rightarrow \text{OAC} + \text{NADH}$

Pentose Phosphate (PP) Pathway

18. $\text{GLUC6P} + 2 \text{NADP} \Rightarrow \text{RIBU5P} + 2 \text{NADPH} + \text{CO}_2$
19. $\text{RIBU5P} \Leftrightarrow \text{RIB5P}$
20. $\text{RIBU5P} \Leftrightarrow \text{XYL5P}$
21. $\text{RIB5P} + \text{XYL5P} \Leftrightarrow \text{SED7P} + \text{GAP}$
22. $\text{SED7P} + \text{GAP} \Leftrightarrow \text{FRUC6P} + \text{E4P}$
23. $\text{XYL5P} + \text{E4P} \Leftrightarrow \text{FRUC6P} + \text{GAP}$

Anaplerotic Routes

Glyoxylate Cycle

24. $\text{ISOCIT} + \text{AcCoA}_{\text{cyt}} \Rightarrow \text{MAL} + \text{SUC}$

Carboxylation of Pyruvate by Enzyme Pyruvate Carboxykinase

25. $\text{PYR} + \text{ATP} + \text{CO}_2 \Rightarrow \text{OAC} + \text{ADP}$

Fermentative Pathways

26. $\text{PYR} \Rightarrow \text{ACET} + \text{CO}_2$
27. $\text{ACET} + \text{NADH} \Leftrightarrow \text{EtOH} + \text{NAD}$
28. $\text{ACET} + \text{NAD} \Leftrightarrow \text{AC} + \text{NADH}$
29. $\text{@ACET} + \text{NADP} \Leftrightarrow \text{AC} + \text{NADPH}$
30. $\text{AC} + 2 \text{ATP} + \text{CoA} \Rightarrow \text{AcCoA}_{\text{cyt}} + 2 \text{ADP}$
31. $\text{GAP} + \text{NADH} \Leftrightarrow \text{GLYC}$

Oxidative Phosphorylation: P/O = 1.09 (Ratio P/O: Stoichiometric of Oxidative Phosphorylation)

32. $2 \text{ NADH} + \text{O}_2 + 2 \text{ PO ADP} \Rightarrow 2 \text{ NAD} + 2 \text{ POATP}$
 33. $2 \text{ FADH}_2 + \text{O}_2 + 2 \text{ PO ADP} \Rightarrow 2 \text{ FAD} + 2 \text{ PO ATP}$

Amino Acids Synthesis

34. $\text{AKG} + \text{NH}_4 + \text{NADPH} \Leftrightarrow \text{GLUT} + \text{NADP}$
 35. $\text{GLUT} + \text{NH}_4 + \text{ATP} \Rightarrow \text{GLUM} + \text{ADP}$
 36. $\text{GLUT} + \text{ATP} + 2 \text{ NADPH} \Rightarrow \text{PRO} + \text{ADP} + 2 \text{ NADP}$
 37. $\text{NH}_4 + \text{ATP} + \text{CO}_2 \Rightarrow \text{CARP} + \text{ADP}$
 38. $2 \text{ GLUT} + \text{AcCoA}_{\text{cyt}} + 4 \text{ ATP} + \text{NADPH} + \text{CARP} + \text{ASP} \Rightarrow \text{ARG} + \text{CoA} + \text{AKG} + \text{AC} + 4 \text{ ADP} + \text{FUM} + \text{NADP}$
 39. $2 \text{ GLUT} + \text{AcCoA}_{\text{cyt}} + 3 \text{ ATP} + 2 \text{ NADPH} + 2 \text{ NAD} \Rightarrow \text{LYS} + \text{CoA} + \text{AKG} + \text{CO}_2 + 3 \text{ ADP} + 2 \text{ NADP} + 2 \text{ NADH}$
 40. $\text{G3P} + \text{GLUT} + \text{NAD} \Rightarrow \text{SER} + \text{AKG} + \text{NADH}$
 41. $\text{SER} + \text{THF} \Leftrightarrow \text{GLY} + \text{METHF}$
 42. $\text{SER} + \text{AcCoA}_{\text{cyt}} + 4 \text{ NADPH} + \text{ATP} \Rightarrow \text{CYS} + \text{AC} + \text{CoA} + 4 \text{ NADP} + \text{ADP}$
 43. $\text{OAC} + \text{GLUT} \Leftrightarrow \text{ASP} + \text{AKG}$
 44. $\text{ASP} + \text{NH}_4 + 2 \text{ ATP} \Rightarrow \text{ASN} + 2 \text{ ADP}$
 45. $\text{ASP} + \text{ATP} + 2 \text{ NADPH} \Rightarrow \text{HOM} + \text{ADP} + 2 \text{ NADP}$
 46. $\text{HOM} + \text{ATP} \Rightarrow \text{THR} + \text{ADP}$
 47. $\text{HOM} + \text{SUCCoA} + \text{CYS} + \text{MYTHF} + \text{ATP} \Rightarrow \text{MET} + \text{CoA} + \text{SUC} + \text{PYR} + \text{NH}_4 + \text{ADP} + \text{THF}$
 48. $\text{THR} + \text{PYR} + \text{NADPH} + \text{GLUT} \Rightarrow \text{ILEU} + \text{NH}_4 + \text{NADP} + \text{CO}_2 + \text{AKG}$
 49. $\text{PYR} + \text{GLUT} \Leftrightarrow \text{ALA} + \text{AKG}$
 50. $2 + \text{PYR} + \text{NADPH} \Rightarrow \text{AKI} + \text{NADP} + \text{CO}_2$
 51. $\text{AKI} + \text{GLUT} \Leftrightarrow \text{VAL} + \text{AKG}$
 52. $@ \text{ AKI} + \text{AcCoA}_{\text{cyt}} + \text{GLUT} + \text{NAD} + \text{ATP} \Rightarrow \text{LEU} + \text{AKG} + \text{CoA} + \text{CO}_2 + \text{NADH} + \text{ADP}$
 53. $\text{PEP} + \text{E4P} + \text{NADPH} + \text{ATP} \Rightarrow \text{CHO} + \text{ADP} + \text{NADP}$
 54. $\text{CHO} + \text{GLUT} \Rightarrow \text{PHEN} + \text{AKG} + \text{CO}_2$
 55. $\text{CHO} + \text{GLUT} + \text{NAD} \Rightarrow \text{TYR} + \text{AKG} + \text{CO}_2 + \text{NADH}$
 56. $\text{CHO} + \text{GLUM} + \text{PRPP} + \text{SER} \Rightarrow \text{TRYP} + \text{CO}_2 + \text{GAP} + \text{GLUT} + \text{PYR}$
 57. $\text{RIB5P} + 2 \text{ ATP} \Rightarrow \text{PRPP} + 2 \text{ ADP}$
 58. $\text{PRPP} + 3 \text{ ATP} + \text{NH}_4 + \text{GLUM} + 2 \text{ NAD} + 2 \text{ NADPH} + \text{CO}_2 \Rightarrow \text{HIS} + 3 \text{ ADP} + 2 \text{ NADH} + \text{NADP} + \text{AKG}$

Nucleotide Biosynthesis

59. $\text{PRPP} + 2 \text{ GLUM} + \text{GLY} + 4 \text{ ATP} + \text{ASP} + 2 \text{ FTHF} + \text{CO}_2 \Rightarrow \text{IMP} + 4 \text{ ADP} + 2 \text{ GLUT} + 2 \text{ THF} + \text{FUM}$
 60. $\text{IMP} + \text{ASP} + \text{ATP} \Rightarrow \text{AMP} + \text{ADP} + \text{FUM}$
 61. $\text{IMP} + \text{NAD} + 2 \text{ ATP} + \text{GLUM} \Rightarrow \text{GMP} + 2 \text{ ADP} + \text{GLUT} + \text{NADH}$
 62. $\text{GLUM} + \text{PRPP} + 2 \text{ ATP} + \text{ASP} + \text{NAD} \Rightarrow \text{UMP} + 2 \text{ ADP} + \text{GLUT} + \text{NADH}$
 63. $\text{UMP} + 2 \text{ ATP} \Leftrightarrow \text{UTP} + 2 \text{ ADP}$
 64. $\text{UTP} + \text{GLUM} + \text{ATP} \Rightarrow \text{CTP} + \text{ADP} + \text{GLUT}$
 65. $\text{CTP} + 2 \text{ ADP} \Leftrightarrow \text{CMP} + 2 \text{ ATP}$

1-Carbon Compound Synthesis

66. $\text{THF} + \text{NADH} + \text{ATP} + \text{CO}_2 \Leftrightarrow \text{FTHF} + \text{NAD} + \text{ADP}$
 67. $\text{THF} + 3 \text{ NADH} + \text{CO}_2 \Leftrightarrow \text{MYTHF} + 3 \text{ NAD}$
 68. $\text{THF} + 2 \text{ NADH} + \text{CO}_2 \Leftrightarrow \text{METHF} + 2 \text{ NAD}$

ATP Consumption for Transport, Maintenance, and Protein Processing

69. $\text{ATP} \Rightarrow \text{ADP}$

Non-Recombinant Protein Synthesis: 4.3 moles ATP / (mole protein-bound amino acid)

- 0.1246ALA + 0.0437ARG + 0.0277ASN + 0.0806ASP + 0.0091CYS + 0.0285GLUM + 0.0820GLUT + 0.0787GLY + 0.0179HIS + 0.0524ILEU + 0.0802LEU + 0.0776LYS + 0.0138MET + 0.0364PHEN + 0.0448PRO + 0.0502SER + 0.0518THR + 0.0076TRYP + 0.0277TYR + 0.0719VAL + 4.3ATP \Rightarrow PROT

Human Superoxide Dismutase (SOD) Synthesis: 4.3 mole ATP / (mole protein-bound amino acid)

- 0.065ALA + 0.026ARG + 0.046ASN + 0.072ASP + 0.026CYS + 0.020GLUM + 0.065GLUT + 0.163GLY + 0.052HIS + 0.059ILEU + 0.059LEU + 0.072LYS + 0.026PHEN + 0.033PRO + 0.065SER + 0.052THR + 0.0065TRYP 0.092VAL + 4.3ATP \Rightarrow SOD

RNA Synthesis: 2.4 moles ATP/ (mole RNA-bound nucleotide)

72. $0.233 \text{ AMP} + 0.233 \text{ GMP} + 0.306 \text{ UMP} + 0.2283 \text{ CMP} + 2.4 \text{ ATP} \Rightarrow \text{RNA}$

Lipid Synthesis

73. $21.6 \text{ AcCoA}_{\text{cyt}} + 0.404 \text{ GAP} + 27.2 \text{ NADPH} + 1.02 \text{ O}_2 + 1.02 \text{ NADH} + 0.278 \text{ SER} \Rightarrow \text{LIPID} + 3.48 \text{ CO}_2$

Carbohydrate Synthesis: Poliglucose (1 ATP/mol carbohydrate-bound glucose-6-P)

74. $\text{GLUC6P} + \text{ATP} \Rightarrow \text{CARBH}$

AcCoA Transport

75. $\text{AcCoA}_{\text{cyt}} \Rightarrow \text{AcCoA}_{\text{mit}}$

Extracellular Transport

76. $\text{CO}_2 \Rightarrow \text{CO}_2^{\text{E}}$
 77. $\text{O}_2^{\text{E}} \Rightarrow \text{O}_2$
 78. $\text{NH}_4^{\text{E}} \Rightarrow \text{NH}_4$

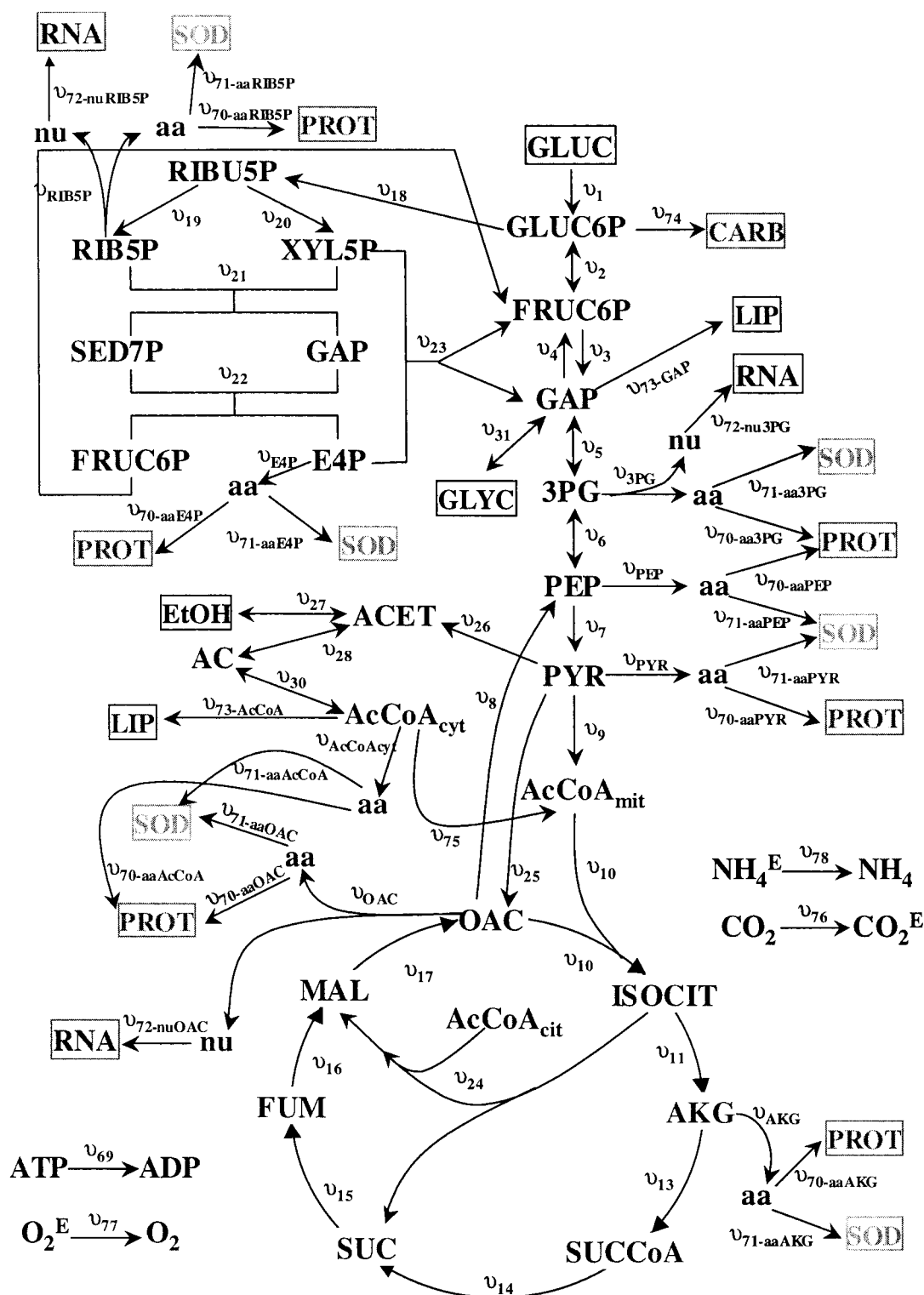


Figure 6. Metabolic fluxes. Synthesis of building blocks from precursor metabolites and their use in the synthesis of macromolecules has been represented by single-step reactions. For example, flux v_{3PG} represents net consumption of $3PG$ for nucleotides (nu) and amino acids (aa) synthesis. Additionally, $v_{71-\text{aa}3PG}$ represents the flux of amino acids obtained from $3PG$ and used in the synthesis of SOD. On the other hand, $v_{70-\text{aa}3PG}$ represents the flux of amino acids obtained from $3PG$ and used in the synthesis of nonrecombinant protein. Finally, $v_{72-\text{nu}3PG}$ represents the flux of nucleotides obtained from $3PG$ and used in the synthesis of RNA. The numbers included in the subscripts represent each reaction as numbered in Appendix A.

Metabolites

1. AC	Acetate	54. NADPH	Nicotinamide adenine dinucleotide phosphate, reduced
2. AcCoA _{cyt}	Cytoplasmic AcCoA	55. NH ₄ ^E	Ammonium, extracellular
3. AcCoA _{mit}	Mitochondrial AcCoA	56. NH ₄	Ammonium
4. ACET	Acetaldehyde	57. O ₂	Oxygen, intracellular
5. ADP	Adenosine-5'-diphosphate	58. O ₂	Oxygen, extracellular
6. AKG	α-ketoglutarate	59. OAC	Oxaloacetate
7. AKI	α-ketoisovalerate	60. PEP	Phosphoenolpyruvate
8. ALA	Alanine	61. PHEN	Phenylalanine
9. AMP	Adenosine-5'-monophosphate	62. PRO	Proline
10. ARG	Arginine	63. PROT	Non-recombinant Protein
11. ASN	Asparagine	64. PRPP	5-phosphoribosil-1-pirophosphate
12. ASP	Aspartate	65. PYR	Pyruvate
13. ATP	Adenosine-5'-triphosphate	66. RIB5P	Ribose-5-phosphate
14. CARBH	Carbohydrates	67. RIBU5P	Ribulose-5-phosphate
15. CARP	Carbamyl phosphate	68. RNA	Ribonucleic Acid
16. CHO	Chorismate	69. SOD	Human Superoxide Dismutase
17. CMP	Citidine-5'-monophosphate	70. SED7P	Sedoheptulose-7-phosphate
18. CO ₂	Carbon Dioxide, intracell.	71. SER	Serine
19. CO ₂	Carbon Dioxide, extracell.	72. SUC	Succinate
20. CoA	Coenzyme A	73. SUCCoA	Succinyl coenzyme A
21. CTP	Citidine-5'-triphosphate	74. THF	Tetrahydrofolate
22. CYS	Cysteine	75. THR	Threonine
23. E4P	Erythrose-4-phosphate	76. TRYP	Tryptophan
24. EtOH	Ethanol	77. TYR	Tyrosine
25. FAD	Flavine adenine dinucleotide	78. UMP	Uridine-5'-monophosphate
26. FADH ₂	Flavine adenine dinucleotide, reduced	79. UTP	Uridine-5'-triphosphate
27. FTHF	Formyl-tetrahydrofolate	80. VAL	Valine
28. FRUC6P	Fructose-6-phosphate	81. XYL5P	Xylulose-5-phosphate
29. FUM	Fumarate		
30. G3P	3-phosphoglycerate		
31. GAP	Glyceraldehyde-3-phosphate		
32. GLUC6P	Glucose-6-phosphate		
33. GLUC	Glucose		
34. GLUM	Glutamine		
35. GLUT	Glutamate		
36. GLY	Glycine		
37. GLYC	Glycerol		
38. GMP	Guanosine-5'-monophosphate		
39. HIS	Histidine		
40. HOM	Homoserine		
41. ILEU	Isoleucine		
42. IMP	Inosine-5'-monophosphate		
43. ISOCIT	Isocitrate		
44. LEU	Leucine		
45. LIPID	Lipids		
46. LYS	Lysine		
47. MAL	Malate		
48. MET	Methionine		
49. METHF	Methylen tetrahydrofolate		
50. MYTHF	Methyl tetrahydrofolate		
51. NAD	Nicotinamide adenine dinucleotide		
52. NADH	Nicotinamide adenine dinucleotide, reduced		
53. NADP	Nicotinamide adenine dinucleotide phosphate		

Figure 6 shows central metabolic reactions considered in the model, as well as pooled reactions for the conversion of precursor metabolites into building blocks, and further use of building blocks to macromolecule biosynthesis. Fluxes of precursor metabolite consumption were calculated considering the stoichiometry of reactions connecting precursor metabolites and building blocks. Fluxes of building blocks consumption consider the stoichiometry of reactions consuming building blocks for the synthesis of nonrecombinant protein, SOD, RNA, carbohydrates, and lipids.

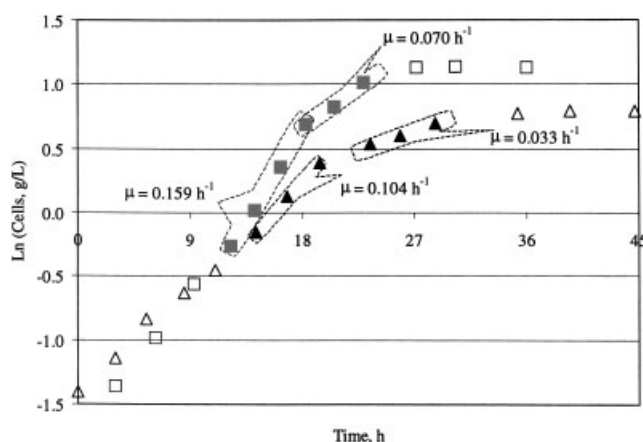


Figure 7. Specific growth rates for recombinant (Δ) and wild-type (\square) strain during exponential growth on glucose and ethanol.

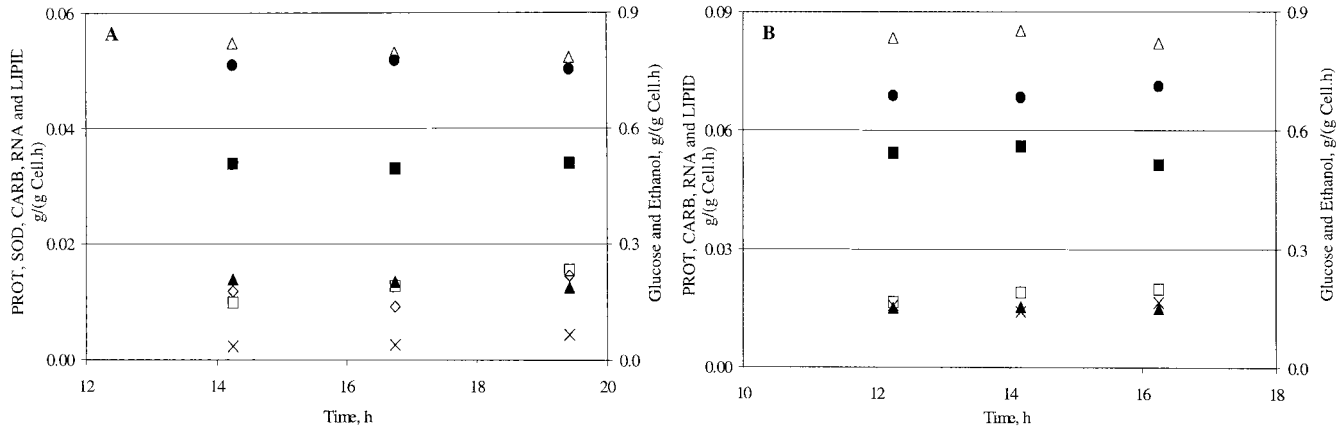


Figure 8. Specific rates for substrate consumption, product formation, and cellular component synthesis during growth on glucose. (A) Recombinant strain, (B) wild type. PROT: total protein, CARB: total carbohydrates, RNA: total RNA, and LIPIDS: Total lipids. (×) Total lipids. Other symbols are as used in Figure 1.

APPENDIX B

Specific Rates

The metabolic fluxes in strains *P+* and *P-* were calculated from the experimental data as “specific growth rates” fluxes. Specific rate of substrate consumption (r_s) and product formation (r_p) were calculated as follows:

$$r_s = -\frac{1}{x} \frac{dc_s}{dt} \quad \text{or} \quad r_p = \frac{1}{x} \frac{dc_p}{dt} \quad (\text{II.1})$$

where x , c_s , and c_p represent the concentration of cells, substrate, and product, respectively. When enough data is available, polynomial fitting could be used to represent experimental data and indeed to calculate specific rates (Papoutsakis and Meyer, 1985; Reardon et al., 1987). The pools of macromolecules composing the cell are defined as its constituents (Stephanopoulos et al., 1998), and in this work include total RNA, total protein (including SOD), total carbohydrates, and total lipids.

In the calculation of specific rates for macromolecular pools, the following expression was used:

$$r_i = \frac{dX_i}{dt} + \mu X_i \quad (\text{II.2})$$

where X_i represents the concentration of i -esim cellular component (mmol/g Cells) and μ the specific growth rate.

Polynomial fitting can also be used in this case, if enough data is available. If exponential growth is considered, and data for two fermentation times are available, the following expression can be obtained from Eq. [2]:

$$\begin{aligned} \frac{dX_i}{dt} &= r_i - \mu X_i \Rightarrow \int_{c_1}^{c_2} \frac{1}{r_i - \mu X_i} dX_i = \int_{t_1}^{t_2} dt \\ -\frac{1}{\mu} \ln \frac{r_i - \mu C_2}{r_i - \mu C_1} &= t_2 - t_1 \\ \Rightarrow r_i &= \frac{\mu (C_2 - C_1 \exp(\mu(t_1 - t_2)))}{1 - \exp(\mu(t_1 - t_2))} \end{aligned} \quad (\text{II.3})$$

The assumption of exponential growth and indeed balanced growth was verified using the experimental data. Figure 7 shows the calculation of specific growth rates of both strains during growth on glucose and ethanol. Figure 8 shows calculated specific rates for recombinant and wild-type strain during growth on glucose. These figures clearly show the existence of balanced growth for both strains. The existence of a stationary phase was verified in both strains by measurements taken at the last three time points. The “entry into stationary phase” is defined as the transition from the last time point of growth on ethanol to the stationary phase. It covers the period from 28.7 h to 35.3 h for the strain *P+* and the period from 22.9 h to 27.2 h for the strain *P-*.